Folding Cooperativity in RNA and DNA Is Dependent on Position in the Helix †

ARTICLE *in* BIOCHEMISTRY · FEBRUARY 2007

Impact Factor: 3.02 · DOI: 10.1021/bi061375l · Source: PubMed

3 AUTHORS, INCLUDING:

Shana Metzger
Georgetown University
10 PUBLICATIONS **182** CITATIONS

SEE PROFILE

Folding Cooperativity in RNA and DNA Is Dependent on Position in the Helix†

Nathan A. Siegfried, Shana L. Metzger, and Philip C. Bevilacqua*

Department of Chemistry, The Pennsylvania State University, University Park, Pennsylvania 16802

Received July 7, 2006; Revised Manuscript Received October 27, 2006

ABSTRACT: Secondary structural motifs play essential roles in the folding and function of RNA and DNA molecules. Previous work from our lab compared the folding of small DNA and RNA hairpin loops containing a sheared GA pair [Moody, E. M., Feerar, J. C., and Bevilacqua, P. C. (2004) *Biochemistry 43*, 7992−7998]. We found that the small DNA hairpins fold in a highly cooperative manner with indirect coupling, while their RNA counterparts fold in a much less cooperative fashion and display direct coupling. Herein, we extend this study to the double-stranded helix. We carried out double mutant cycles on base pairs having identical nearest-neighbor contexts but located in either external or internal helical registers. In the external register, both RNA and DNA exhibit extensive folding cooperativity between the penultimate and terminal base pair, which is independent of mismatch identity. In contrast, DNA exhibits virtually no folding cooperativity in the center of the helix, while RNA maintains substantial coupling, which is dependent on mismatch identity. Two models account for these non-nearest-neighbor effects: one involves the unfavorable entropy of helix initiation common to DNA and RNA, and the other involves steric and electrostatic strain peculiar to RNA. These data show that RNA can display cooperativity less than, greater than, or equal to that of DNA depending on context and position.

RNA and DNA can assume complex three-dimensional structures that lead to diverse functions such as ligand binding, gene regulation, and catalysis (*1*, *2*). These structures often undergo conformational changes during their reactions. Fully understanding the function of RNA and DNA therefore requires a fundamental understanding of RNA and DNA folding pathways. Folding of RNA is typically, although not exclusively, hierarchical in nature, with secondary structure preceding tertiary structure (*3*, *4*). This suggests that RNA secondary structures may play a fundamental role in affecting the energetics and functions of RNA tertiary structures. Indeed, secondary structural elements are key recognition features in riboswitches (*1*) and fundamental biological processes involving small RNAs (*5*). In addition, RNA secondary structures are often responsible for misfolding in large RNAs (*6*−*10*). As such, tremendous interest in the thermodynamics that govern RNA and DNA secondary structure formation has been generated (*11*).

The folding of RNA and DNA is most commonly treated with the nearest-neighbor model (*12*, *13*). This formalism provides a convenient and, in many cases, effective treatment of RNA and DNA folding. In this model, the total free energy for folding is treated as a summation of smaller terms, each of which can be determined empirically (*14*). Using this model, the free energy changes associated with an array of secondary structural motifs have been determined, including helical bulges, internal loops, and hairpin loops (*11*−*13*). Despite the many successes of this approach, it does have certain limitations. First, free energy terms may depend on the position in the helix. To determine individual free energy terms experimentally, motifs of interest are typically placed in the center of a helix (*12*, *13*). While generally effective, this approach does not account for helix end effects. For instance, the free energy of a RNA mismatch with identical nearest-neighbor contexts[1] has been shown to depend on the distance to a helix end, a so-called "non-nearest-neighbor" effect (*15*). Second, the molecular origins of free energy effects are not revealed. For instance, the effect of a helical defect, such as an internal loop, on weakening a neighboring base pair(s) is generally not parsed out. One goal of this study is to test whether there is a relationship between the dependence of free energy on helix position and the nonadditivity of interactions.

The energetic effect of one interaction on a neighboring interaction is termed nonadditivity, or folding cooperativity (*16*−*19*). Nonadditivity is often analyzed by double and triple mutant cycles (*20*). For example, deletion of a functional group engaged in a single hydrogen bond may weaken neighboring hydrogen bonds and stacking interactions. Interactions that have been lost due to the first deletion cannot be removed in subsequent functional group deletions. In this scenario, the observed energetic effect for the first deletion

† Supported by NSF Grant MCB-9984129.

* To whom correspondence should be addressed. Phone: (814) 863-3812. Fax: (814) 863-8403. E-mail: pcb@chem.psu.edu.

[1] Abbreviations: context, identity of nearest neighbors to a given base pair; δ_{AB}, coupling free energy between positions A and B; DM, double mutant DNA or RNA oligonucleotide with both the single AT to mismatch and the GC to IC change; EDTA, ethylenediaminetetraacetic acid; Ext, external register; HS, high-salt 114 mM ionic strength conditions; I, inosine; IC, DNA or RNA oligonucleotide with a single GC to IC change; Int, internal register; LS, low-salt 14 mM ionic strength conditions; MM, mismatch region of an RNA or DNA oligonucleotide in which two identical bases are across from each other, resulting from an AT or AU to AA, GG, or UU change; $P_{10}E_{0.1}$, 10 mM sodium phosphate and 0.1 mM Na_2EDTA (pH 7.0); position, location of a mismatch relative to the base of the hairpin; T_M, melting temperature; WT, wild-type fully paired DNA or RNA oligonucleotide.

10.1021/bi061375l CCC: $37.00
Published on Web 01/02/2007

can be larger than the intrinsic energetic value of the particular interactions of that functional group, while the observed energetic effects for subsequent deletions can be smaller than their intrinsic energetic values. There are many instances where it is helpful to understand nonadditivity effects. For example, it could provide insight into the molecular causes of energetic effects of naturally occurring helical defects and site-directed mutations on RNA and DNA enzyme function (*18*, *19*), or the ability of a protein to bind RNA or DNA (*21*). In addition, nonadditive effects could impact RNA and DNA structure prediction (*11*) and understanding of the intrinsic energetic values of hydrogen bonding and stacking (*22*−*24*).

We previously used double and triple mutant cycles to study the folding of DNA hairpins with triloops and expanded triloops containing sheared GA pairs (*24*, *25*). Results supported a model in which these loops have a highly cooperative network of interactions. Subsequently, it was demonstrated that these DNA loops fold more cooperatively than their RNA counterparts (*26*). The RNA loops have a much more extensive network of interactions than the DNA loops. As such, the molecular origin of the cooperativity was attributed to the DNA being easily collapsed upon deletion of a single functional group, and the RNA not collapsing upon loss of a few functionalities (*26*). Since nonadditivity is context-dependent, other secondary structural motifs may behave differently. In this study, we compare the nonadditivity of RNA and DNA folding in different positions within the double-stranded helix but in otherwise identical nearest-neighbor contexts. Implications of these findings on various biochemical topics, including RNA and DNA structure prediction, are discussed.

MATERIALS AND METHODS

Preparation of DNA and RNA. Synthetic DNA (IDT DNA, Coralville, IA) and RNA (Dharmacon Inc., Lafayette, CO) oligonucleotides were used in this study. Oligonucleotides were desalted by dialysis against sterile deionized water for 6 h with a flow rate of ~3 mL/min using an eight-well microdialysis system (Gibco-BRL Life Technologies). Purity was confirmed as described in the Supporting Information.

Mass spectroscopy data were acquired to confirm authenticity and purity. Agreement between calculated and measured molecular masses was excellent. The presence of a single band by PAGE combined with the proper molecular weight supported the high purity and authenticity of the samples (see the Supporting Information).

UV Melting Experiments. Thermodynamic parameters are from UV melting experiments performed in 10 mM sodium phosphate and 0.1 mM Na_2EDTA (pH 7.0) ($P_{10}E_{0.1}$), which results in a total Na^+ concentration of 14 mM. In some experiments, 100 mM KCl was added to increase the ionic strength; this mixture of sodium and potassium ions closely mimics the monovalent ion composition inside a typical mammalian cell (*27*). The melt data were fit to a two-state model with sloping baselines and analyzed using a Marquadt algorithm for nonlinear curve fitting in Kaleidagraph version 3.5 (Synergy Software). The fit provided ΔH and T_M values directly, as well as slopes and intercepts for baselines. ΔS was calculated from the relation $\Delta S = \Delta H/T_M$, and ΔG was calculated from the relation $\Delta G = \Delta H(1 - T/T_M)$. DNA parameters are averages of results from experiments with three or more independently prepared samples at concentrations ranging from 5 to 25 μM. RNA parameters are averages of three or more independently prepared samples ranging from 1 to 25 μM. Similarity among T_M values resulting from melts at these different concentrations was consistent with the unfolding transition being from the hairpin species. Certain high-concentration RNA experiments revealed an overlapping low-temperature transition, and these melts were excluded from the analysis.

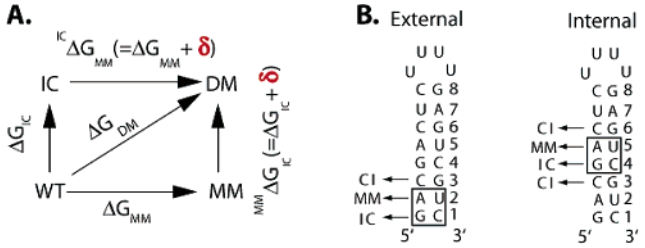

FIGURE 1: (A) Thermodynamic box for a double mutant cycle. ΔG_A is the free energy change associated with mutation A, and ${}^B\Delta G_A$ is ΔG_A in the background of mutation B. WT is the wild-type sequence. MM is the AU to mismatch change. IC is the GC to IC change. DM is the double mutant with both changes. δ is the coupling free energy and represents nonadditivity. (B) Secondary structures for RNA oligonucleotides. Mutations are shown, and registers having identical nearest-neighbor contexts are boxed. "External" denotes a helix with the mutational register at the terminus of the helix, and "Internal" denotes a helix with the mutational register near the middle of the helix. The sequence for DNA is identical to RNA except U's are changed to T's. Base pairs are numbered from the base of the helix.

To favor the hairpin conformation, oligonucleotides were renatured prior to each melt by being heated to 99 °C for 1 min in the spectrometer, followed immediately by a UV melting experiment from 95 to 5 °C. Subsequent UV melts from 5 to 95 °C and from 95 to 5 °C were carried out in succession, and overlapping curves were obtained consistent with the reversibility of the transition. UV absorbance melting profiles were acquired at either 260 or 280 nm and gave similar parameters. Cuvettes with path lengths of 1, 5, and 10 mm were used, with data collected every 0.5 °C on a Gilford Response II spectrophotometer equipped with a temperature controller. Concentrations were determined using absorbance values of the unfolded state at 95 °C, and extinction coefficients were determined from a nearest-neighbor analysis. Representative melting profiles are shown in the Supporting Information.

Analysis of Double Mutant Cycles. The additivity of $\Delta G°_{37}$ values was analyzed as described previously (*16*, *17*, *20*, *24*−*26*). The free energy change associated with mutation of AT or AU to a given mismatch (MM) is denoted ΔG_{MM}. The change associated with mutation of GC to IC is denoted with ΔG_{IC}. The change associated with both mutations is denoted with ΔG_{DM} for double mutant. The change associated with mutation A in the presence of mutation B is denoted ${}^B\Delta G_A$ (Figure 1A). The magnitude of the nonadditive, or coupling, effect between the two mutated base pairs, A and B, is the coupling free energy, δ_{AB}, which was calculated according to the equations

$$\delta_{AB} = \Delta G°_{37}(\mathrm{WT}) + \Delta G°_{37}(\mathrm{DM}) - [\Delta G°_{37}(\mathrm{MM}) + \Delta G°_{37}(\mathrm{IC})] \quad (1a)$$

$$\delta_{AB} = \Delta G_{AB}(DM) - [\Delta G_A(MM) + \Delta G_B(IC)] \quad (1b)$$

A negative value for δ indicates that deleting the first interaction weakens the second and signifies positive coupling between functional groups (*16*). A positive value of δ indicates that deleting the first interaction strengthens the second and signifies negative coupling. A δ value of 0 supports no coupling. A double mutant is considered "completely nonadditive" if $-\delta$ equals the smaller of ΔG_{MM} or ΔG_{IC}, which causes either ${}^{IC}\Delta G_{MM}$ or ${}^{MM}\Delta G_{IC}$ to approach zero (*25*). The percent effect (see Table 2) is calculated as the ratio of $-\delta_{AB}$ to the smaller of ΔG_{MM} or ΔG_{IC} and represents the magnitude of the coupling energy relative to the smaller energetic impact of a single mutation.

Error Analysis. Errors were propagated into the two-state model described above. Details are provided in the Supporting Information.

RESULTS

Oligonucleotide Design and Rationale. The oligonucleotides used in this study are 20mers with a core nearest-neighbor sequence that is invariant between DNA and RNA, other than the fact that T was replaced with U (Figure 1B). The core hairpin has a fully paired perfect helix, while mutant species bear AT to MM, GC to IC, or both mutations, where I is inosine. Mutational registers with identical nearest-neighbor contexts were placed in internal or external registers within the helix (Figure 1B). Identical nearest-neighbor contexts facilitate direct comparison of effects of internal and external helical positions on double mutant cycles. Initial coupling studies were between the AU base pair and the GC base pair below it, probed by AU to AA and GC to IC changes. Additional studies were conducted for RNA on the CG base pair above the AU pair in both external and internal positions, as well as the next-nearest-neighbor CG base pair. In addition, the RNA mismatch was varied to UU or GG, and external and internal coupling free energies were examined.

A loop of U_4 was chosen because it is a relatively unstructured and unstable loop (*28*, *29*), which facilitates two-state melting and a T_M that allows for a full upper baseline. The AT to AA and GC to IC combination was chosen because it allows the effects of a mismatch substitution (AT to AA) on neighboring interactions to be assessed by a minimal functional group change: the GC to IC mutation involves removal of the amino group, which changes a three-hydrogen bond base pair to a two-hydrogen bond one. The AA to AT change may bear similarity to AC to wobble A^+·C changes that occur upon proton loading and pK_a shifting (*30*). The UU and GG mismatches were chosen because there are thermodynamic (*15*) and structural studies (*31*, *32*) published on these two mismatches and because they add breadth to the study. We also assessed coupling at different salt concentrations to test the importance of electrostatics.

Cooperativity in Double-Stranded DNA Is Dependent on Helical Position. To test the dependence of cooperativity on helical position, we determined δ values for DNA constructs with internal and external mutational registers but otherwise identical nearest-neighbor contexts. (This section focuses on the low-ionic strength results, with the effect of increasing ionic strength considered in a subsequent section.) Parameters for each oligonucleotide are provided in Table 1, and coupling free energies (δ values) are listed in Table 2.

For DNA, external registers displayed greater cooperativity (i.e., more negative δ values) than internal registers (Figure 2). Mutation of the AT base pair to an AA mismatch resulted in substantial destabilization in both helical positions (ΔG_{AA} is 2.18 and 3.34 kcal/mol for base pairs 2 and 5, respectively). In the external register, a subsequent change of the terminal GC pair to an IC pair resulted in a very small change in stability (0.05 kcal/mol), suggesting that the terminal base pair is formed only when the penultimate pair is formed. In addition, δ_{12} was large (-0.82 kcal/mol) as was the percent effect at 94% (Table 2), signifying complete nonadditivity.

The internal DNA register, on the other hand, exhibited a significant effect for the subsequent GC to IC change at position 4 of 1.63 kcal/mol. This gives an internal δ_{45} of only -0.38 kcal/mol, or 19%, suggesting that disruption of the internal AT base pair only slightly weakens the neighboring GC base pair if at all. Apparently, nonadditivity is highly dependent on position within double-stranded DNA. Surprisingly, despite the larger nonadditivity of the external register, the AT to AA and GC to IC single mutant changes revealed significantly larger ($\sim$1.2 kcal/mol each) thermodynamic penalties in the internal register. This phenomenon likely reflects fraying near the terminus of the helix, which reduces the intrinsic stability of the terminal and penultimate base pairs (see the Discussion).

Cooperativity in Double-Stranded RNA Is High in both External and Internal Helical Positions. Examination of δ_{12} values from RNA external cycles revealed percent cooperativity patterns similar to those for DNA. The percent effect for RNA at the terminus was 117%, similar to the value of 94% for DNA and signifying complete nonadditivity for both nucleic acids near the terminus (Table 2). While the percent effects were similar, magnitudes of the coupling free energies were approximately 2 times larger for RNA than for DNA. RNA and DNA had δ_{12} values of -1.68 and -0.82 kcal/mol, respectively. Larger coupling free energies in RNA are consistent with local interactions generally being more stable in RNA than in DNA (*12*, *13*). Observation of large percent effects in the external position for both RNA and DNA is suggestive of a common molecular basis (see the Discussion).

In contrast to DNA, internal registers in RNA also exhibited significant nonadditivity. δ_{45} for the internal RNA register was -1.73 (50%), which is similar in magnitude to the external RNA register effect (δ_{12}) of -1.68 kcal/mol. Because RNA was unique in displaying cooperativity internally, we investigated other coupling networks as well. Coupling between the AU base pair at position 5 and the CG base pair above it at position 6 was found to be significant with a δ_{56} of -0.85 kcal/mol.

To see whether coupling extended beyond neighboring base pairs, a double mutant cycle was conducted between positions 5 and 3. Coupling between the AU base pair at position 5 and the next-nearest-neighbor CG base pair at position 3 was still significant with a δ_{35} of -0.79 kcal/mol. Apparently, changing the base pair at position 5 from an AU pair to an AA pair has effects that extend beyond its nearest neighbors, a so-called non-nearest-neighbor effect. Last, we tested whether coupling extends upward in the external register. A double mutant cycle was conducted between positions 2 and 3. Coupling between the AU base

Table 1: Thermodynamic Parameters for Folding of WT, AA, IC, and DM DNA and RNA at Low and High Ionic Strengths

sequence[a]	base pair	ionic strength (mM)	T_M (°C)	$\Delta H°$ (kcal/mol)	$\Delta S°$ (eu)	$\Delta G°_{37}$ (kcal/mol)
			DNA			
WT		114	75.9 ± 0.07	−61.1 ± 0.63	−175 ± 1.8	−6.80 ± 0.07
Ext AA	2	114	71.0 ± 0.06	−54.1 ± 0.50	−157 ± 1.5	−5.34 ± 0.05
Ext IC	1	114	74.4 ± 0.05	−60.1 ± 0.53	−173 ± 1.5	−6.46 ± 0.06
Ext DM	1,2	114	70.8 ± 0.05	−53.4 ± 0.44	−155 ± 1.3	−5.25 ± 0.04
Int AA	5	114	61.7 ± 0.07	−56.2 ± 0.53	−168 ± 1.6	−4.14 ± 0.04
Int IC	4	114	67.6 ± 0.03	−61.2 ± 0.39	−180 ± 1.2	−5.50 ± 0.03
Int DM	4,5	114	52.2 ± 0.05	−49.3 ± 0.43	−151 ± 1.4	−2.30 ± 0.02
WT		14	67.8 ± 0.03	−67.8 ± 0.51	−199 ± 1.5	−6.13 ± 0.05
Ext AA	2	14	61.7 ± 0.05	−53.5 ± 0.40	−160 ± 1.2	−3.95 ± 0.03
Ext IC	1	14	65.9 ± 0.04	−61.6 ± 0.46	−182 ± 1.4	−5.26 ± 0.04
Ext DM	1,2	14	61.5 ± 0.05	−53.3 ± 0.41	−159 ± 1.2	−3.90 ± 0.03
Int AA	5	14	53.6 ± 0.09	−55.2 ± 0.78	−169 ± 2.4	−2.79 ± 0.04
Int IC	4	14	59.9 ± 0.06	−60.1 ± 0.53	−180 ± 1.6	−4.12 ± 0.04
Int DM	4,5	14	44.0 ± 0.07	−52.5 ± 0.64	−166 ± 2.1	−1.16 ± 0.01
			RNA			
WT		114	82.4 ± 0.05	−73.8 ± 0.59	−208 ± 1.7	−9.43 ± 0.08
Ext AA	2	114	79.0 ± 0.04	−66.0 ± 0.54	−187 ± 1.6	−7.88 ± 0.06
Ext IC	1	114	80.6 ± 0.07	−65.7 ± 0.58	−186 ± 1.7	−8.10 ± 0.07
Ext DM	1,2	114	79.1 ± 0.07	−62.4 ± 0.62	−177 ± 1.8	−7.46 ± 0.07
Int AA	5	114	65.1 ± 0.03	−59.1 ± 0.37	−175 ± 1.1	−4.92 ± 0.03
Int IC	4	114	72.6 ± 0.04	−61.4 ± 0.44	−178 ± 1.3	−6.32 ± 0.05
Int DM	4,5	114	55.9 ± 0.03	−50.0 ± 0.22	−152 ± 0.69	−2.87 ± 0.01
WT		14	75.6 ± 0.03	−75.8 ± 0.58	−217 ± 1.7	−8.39 ± 0.06
Ext AA	2	14	71.6 ± 0.04	−65.7 ± 0.58	−191 ± 1.7	−6.59 ± 0.06
Ext IC	1	14	72.6 ± 0.4	−67.4 ± 0.64	−195 ± 1.9	−6.95 ± 0.06
Ext DM	1,2	14	71.4 ± 0.06	−68.4 ± 1.2	−199 ± 3.4	−6.83 ± 0.12
Ext CI	3	14	68.8 ± 0.03	−65.1 ± 0.33	−190 ± 1.0	−6.05 ± 0.03
Ext DM	2,3	14	67.6 ± 0.04	−59.8 ± 0.44	−175 ± 1.3	−5.37 ± 0.04
Int AA	5	14	58.9 ± 0.03	−56.3 ± 0.34	−169 ± 1.0	−3.71 ± 0.02
Int IC	4	14	65.6 ± 0.03	−58.6 ± 0.27	−173 ± 0.81	−4.95 ± 0.02
Int DM	4,5	14	49.6 ± 0.02	−50.9 ± 0.22	−158 ± 0.68	−2.00 ± 0.01
Int CI	6	14	67.3 ± 0.09	−64.9 ± 0.69	−191 ± 2.1	−5.76 ± 0.06
Int DM	5,6	14	49.8 ± 0.10	−48.8 ± 0.78	−151 ± 2.5	−1.93 ± 0.03
Int DM	3,5	14	51.1 ± 0.09	−49.8 ± 0.58	−154 ± 1.8	−2.16 ± 0.03

[a] Error propagation is described in the Supporting Information.

Table 2: Free Energy Parameters and δ Values for AA Double Mutant Cycles

sequence	ΔG_{AA}	ΔG_{IC}	ΔG_{DM}	ΔG_{DM}(add)[a]	δ_{AB}	δ_{AB}[b]	% effect[c]
dExt LS[d]	2.18	0.87	2.23	3.05	δ_{12}	−0.82 ± 0.1	94
dExt HS	1.46	0.34	1.55	1.80	δ_{12}	−0.25 ± 0.1	74
dInt LS	3.34	2.01	4.97	5.35	δ_{45}	−0.38 ± 0.1	19
dInt HS	2.66	1.30	4.50	3.96	δ_{45}	0.54 ± 0.1	−42
rExt LS	1.80	1.44	1.56	3.24	δ_{12}	−1.68 ± 0.1	117
rExt LS	1.80	2.34	3.02	4.14	δ_{23}	−1.12 ± 0.1	62
rExt HS	1.55	1.33	1.97	2.88	δ_{12}	−0.91 ± 0.1	68
rInt LS	4.68	3.44	6.39	8.12	δ_{45}	−1.73 ± 0.1	50
rInt LS	4.68	2.63	6.46	7.31	δ_{56}	−0.85 ± 0.1	32
rInt LS	4.68	2.34	6.23	7.02	δ_{35}	−0.79 ± 0.08	34
rInt HS	4.51	3.11	6.56	7.62	δ_{45}	−1.06 ± 0.1	34

[a] ΔG from WT to DM if ΔG_{AA} and ΔG_{IC} were additive. [b] δ values were calculated as the difference between columns 4 and 5. Errors were propagated from eq 1a. Errors in free energies for the preceding four columns are slightly less and are estimated to be ±0.1 kcal/mol. [c] The percent effect is calculated as the ratio of $-\delta_{AB}$ to the smaller of ΔG_{AA} or ΔG_{IC}. [d] All values are at 37 °C in units of kilocalories per mole. Error propagation is described in the Supporting Information.

pair at position 2 and the CG base pair at position 3 was significant with a δ_{23} of −1.12 kcal/mol.

Dependence of Coupling on Mismatch Identity: UU and GG Mismatches. The studies presented thus far examined the coupling free energy between various base pairs as AA and IC mismatches were introduced into oligonucleotides. To determine if the observed effects were unique to AA mismatches, UU and GG mismatches were introduced adjacent to an IC pair in both external and internal helical positions in the background of RNA under low-salt conditions (Tables 3 and 4 and Figure 3).

In the external position, the UU and GG mismatches acted like the AA mismatch, with percent couplings for δ_{12} of 117, 86, and 117% for AA, UU, and GG, respectively (Table 4). Moreover, in the external position, the thermodynamic penalty associated with introduction of the mismatch, ΔG_{MM}, took on similar values of 1.80, 1.65, and 1.41 kcal/mol for AA, UU, and GG, respectively (Table 4). These observations are consistent with a molecular basis for coupling between the penultimate mismatch and the terminal base pair that is independent of mismatch identity (see the Discussion).

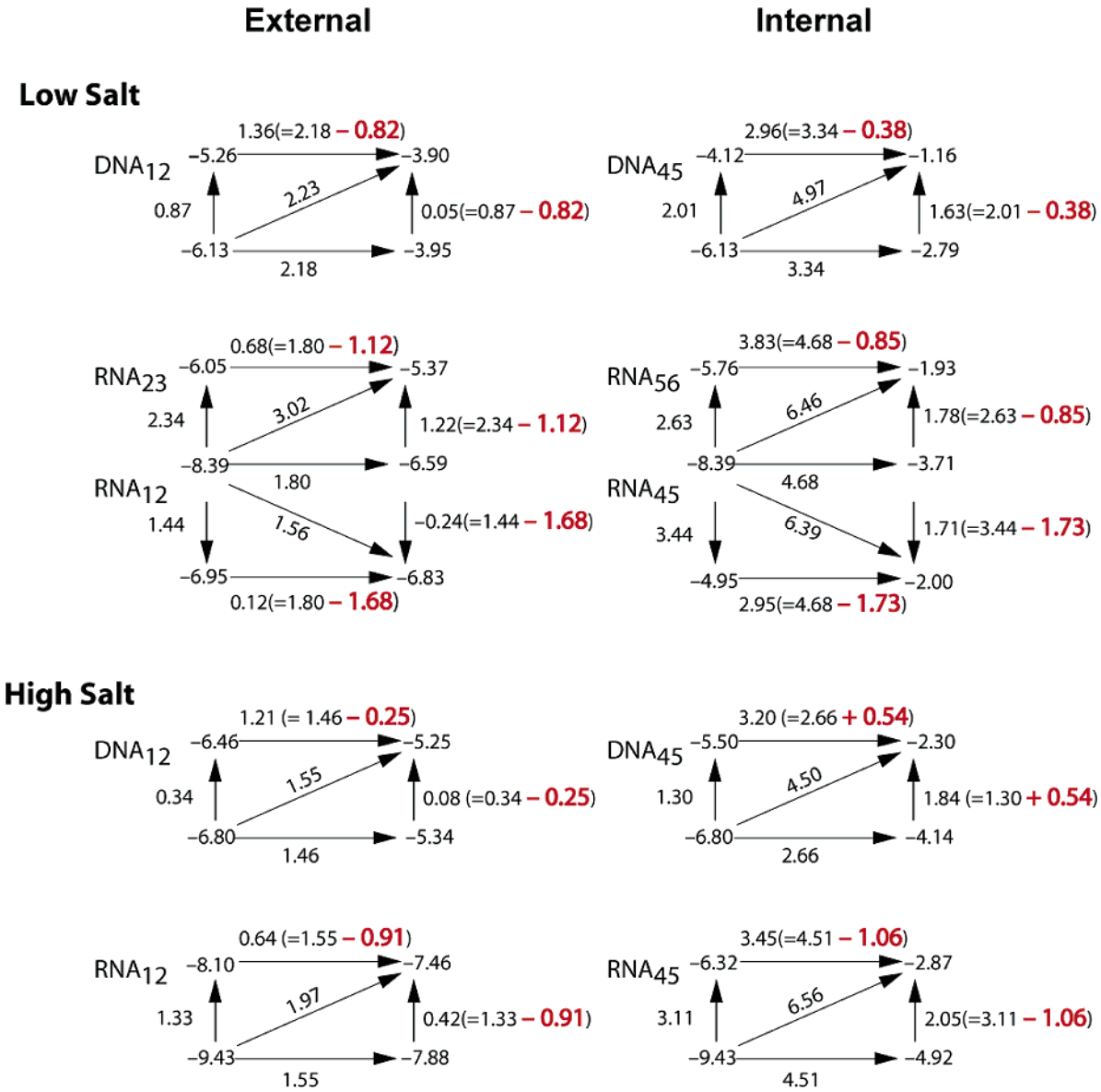

FIGURE 2: Thermodynamic boxes for low-salt (top) and high-salt (bottom) conditions for DNA and RNA sequences in both external and internal registers with an AA mismatch. The magnitude of the cooperativity of the system is represented by the number in red, as described in the legend of Figure 1. Cycles that share a common AU base pair were joined into double boxes.

Table 3: Thermodynamic Parameters for Folding of WT, GG, UU, IC, and DM RNA at Low Ionic Strengths

sequence[a]	base pair	ionic strength (mM)	T_M (°C)	$\Delta H°$ (kcal/mol)	$\Delta S°$ (eu)	$\Delta G°_{37}$ (kcal/mol)
WT		14	75.6 ± 0.03	−75.8 ± 0.58	−217 ± 1.7	−8.39 ± 0.06
Ext UU[a]	2	14	71.3 ± 0.07	−67.7 ± 0.87	−196 ± 2.6	−6.74 ± 0.09
Ext IC	1	14	72.6 ± 0.4	−67.4 ± 0.64	−195 ± 1.9	−6.95 ± 0.06
Ext DM	1,2	14	71.3 ± 0.04	−65.7 ± 0.60	−191 ± 1.8	−6.54 ± 0.06
Int UU	5	14	61.3 ± 0.03	−70.2 ± 0.50	−210 ± 1.5	−5.11 ± 0.04
Int IC	4	14	65.6 ± 0.03	−58.6 ± 0.27	−173 ± 0.81	−4.95 ± 0.02
Int DM	4,5	14	53.2 ± 0.05	−51.1 ± 0.38	−157 ± 1.2	−2.53 ± 0.02
WT		14	75.6 ± 0.03	−75.8 ± 0.58	−217 ± 1.7	−8.39 ± 0.06
Ext GG	2	14	72.9 ± 0.08	−67.3 ± 0.68	−194 ± 2.0	−6.98 ± 0.07
Ext IC	1	14	72.6 ± 0.4	−67.4 ± 0.64	−195 ± 1.9	−6.95 ± 0.06
Ext DM	1,2	14	72.8 ± 0.08	−69.5 ± 0.85	−201 ± 2.5	−7.19 ± 0.09
Int GG	5	14	66.0 ± 0.03	−72.0 ± 0.40	−212 ± 1.2	−6.15 ± 0.03
Int IC	4	14	65.6 ± 0.03	−58.6 ± 0.27	−173 ± 0.81	−4.95 ± 0.02
Int DM	4,5	14	56.9 ± 0.05	−55.2 ± 0.45	−167 ± 1.4	−3.33 ± 0.03

[a] Error propagation is described in the Supporting Information.

In the internal position, the thermodynamic effects of the UU and GG base pairs differed somewhat from that of the AA base pair. The coupling free energies for the internal position (δ_{45}) were −1.73, −0.86, and −0.62 kcal/mol for AA, UU, and GG, respectively (Table 4). The ΔG_{MM} values in the internal position were 4.68, 3.28, and 2.24 kcal/mol for AA, UU, and GG mismatches, respectively (Table 4). These findings are consistent with those of Kierzek et al.

Table 4: Free Energy Parameters and δ Values for All RNA Mismatch Double Mutant Cycles at Low Salt Concentrations

sequence	ΔG_{MM}	ΔG_{IC}	ΔG_{DM}	ΔG_{DM}(add)[a]	δ_{AB}	δ_{AB}[b]	% effect[c]
rExt AA[d]	1.80	1.44	1.56	3.24	δ_{12}	-1.68 ± 0.1	117
rInt AA	4.68	3.44	6.39	8.12	δ_{45}	-1.73 ± 0.1	50
rExt UU	1.65	1.44	1.85	3.09	δ_{12}	-1.24 ± 0.2	86
rInt UU	3.28	3.44	5.86	6.72	δ_{45}	-0.86 ± 0.1	26
rExt GG	1.41	1.44	1.20	2.85	δ_{12}	-1.65 ± 0.1	117
rInt GG	2.24	3.44	5.06	5.68	δ_{45}	-0.62 ± 0.1	28

[a] ΔG from WT to DM if ΔG_{MM} and ΔG_{IC} were additive. [b] δ values were calculated as the difference between columns 4 and 5. Errors were propagated from eq 1a. Errors in free energies for the preceding four columns are slightly less and are estimated to be ± 0.1 kcal/mol. [c] The percent effect is calculated as the ratio of $-\delta_{AB}$ to the smaller of ΔG_{MM} or ΔG_{IC}. [d] AA, UU, and GG refer to the mismatch found in the double mutant cycles. Values for AA are also found in Table 2. All values are at 37 °C in units of kilocalories per mole. Error propagation is described in the Supporting Information.

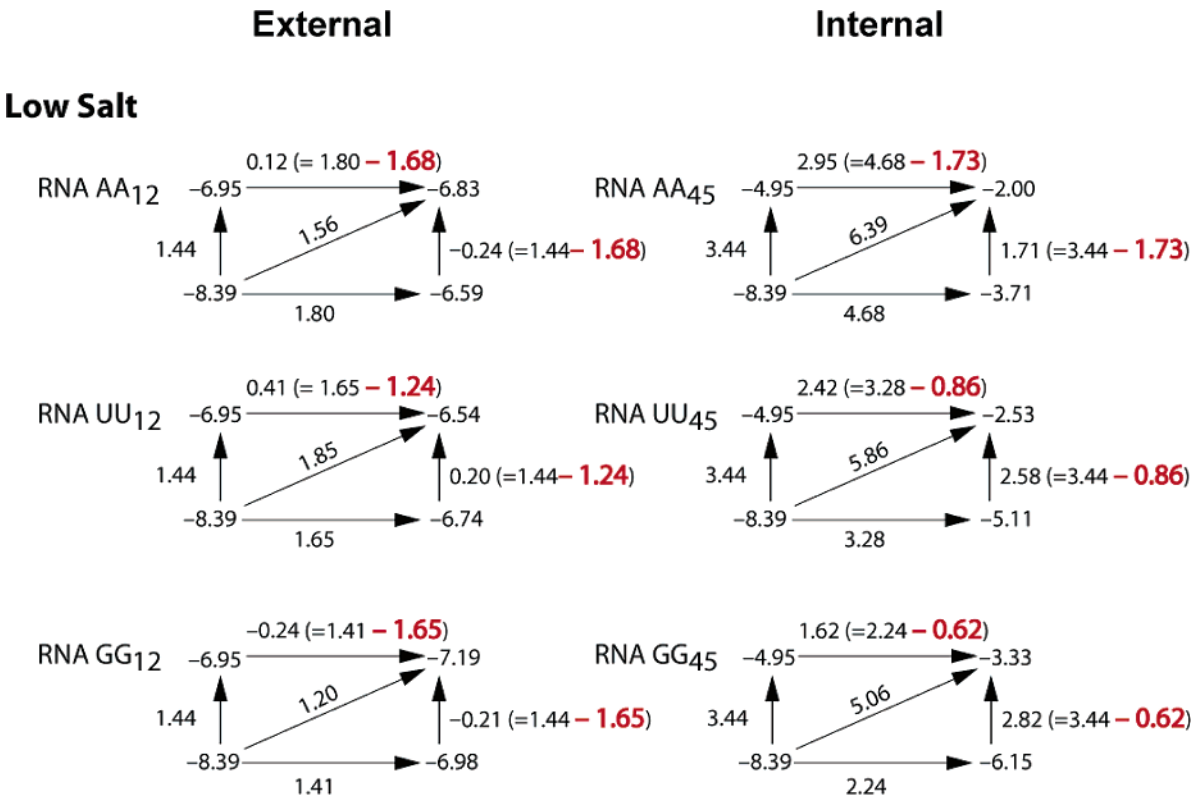

FIGURE 3: Thermodynamic boxes for low-salt conditions for RNA sequences in both internal and external registers for all three mismatches: AA, UU, and GG. The magnitude of the cooperativity of the system is represented by the number in red, as described in the legend of Figure 1.

(*15*) in that the stability of the GG mismatch is essentially unaffected by its position within a helix ($\Delta G_{int-ext} = 0.83$ kcal/mol), while the UU and AA mismatches are substantially more destabilizing internally than externally, with $\Delta G_{int-ext}$ values of 1.63 and 2.88 kcal/mol, respectively (Table 4).

The disparate effects of the three mismatches can be understood structurally from NMR studies in that the GG mismatch is known to form a two-hydrogen bond *syn*−*anti* base pair that is largely compatible with an A-form Watson−Crick duplex (*32*); consequently, there is a minimal perturbation of this mismatch on the strength of neighboring pairs and hence on cooperativity. NMR studies revealed that the UU mismatch forms a base pair with one direct hydrogen bond and one water-mediated hydrogen bond, which is likely to distort the helix from its normal A-form geometry (*31*) more than the GG mismatch. This is consistent with a greater perturbation of the UU mismatch than the GG mismatch on the strength of neighboring pairs, hence leading to larger cooperativity. There are no reported structures for an AA mismatch flanked by Watson−Crick base pairs in the noncanonical database (*33*). However, the strong position dependence of the AA mismatch is fully compatible with our initial interpretation that this mismatch has a substantial and long-range perturbation on neighboring structure and hence the largest cooperativity.

Effect of Ionic Strength on Cooperativity in RNA and DNA. In an effort to determine the electrostatic component of the energetics, we remeasured the double mutant cycles in internal and external registers for both RNA and DNA at higher ionic strengths. Increasing the ionic strength from 14 to 114 mM significantly diminished the energetic consequences of single DNA changes. In particular, the AT to AA change was on average 0.7 kcal/mol less destabilizing at 114 mM, while the GC to IC change was on average 0.6 kcal/mol less destabilizing (Table 2); in general, these effects

were independent of helix position. In contrast, increasing the ionic strength had only minimal energetic consequences on the single mutants in RNA. In particular, the AU to AA and GC to IC changes were only 0.2 kcal/mol less destabilizing at high ionic strengths in both internal and external positions.

Next, we considered the effect of ionic strength on the coupling free energies. The external register in DNA remained highly nonadditive at higher ionic strengths, with percent effects decreasing slightly from 94 to 74% when the ionic strength increased from 14 to 114 mM. On the other hand, the percent effects on the coupling free energies for the internal register in DNA changed from 19 to −42% when the ionic strength increased. The negative percent effect is associated with a positive δ and negative coupling and is indicative of an energetic compensation in which deletion of one interaction strengthens another.

In the case of RNA, both registers showed somewhat weakened coupling at higher ionic strengths, although overall coupling remained significant. For the external register, increasing the ionic strength caused the percent effect to change from 117 to 68%, while increasing the ionic strength led the percent effect to change from 50 to 34% for the internal register. For both external and internal registers in RNA, the magnitude of the coupling free energy remained significant at higher ionic strengths, with values of −0.91 and −1.06 kcal/mol, respectively.

DISCUSSION

Extensive nearest-neighbor studies have been carried out on RNA and DNA, and these have led to significant advances in the prediction of structure from sequence (*11*−*13*). Interestingly, several studies from the Turner lab have uncovered non-nearest-neighbor effects for certain motifs. These include a dependence of the free energy of tandem GU mismatches on flanking base pairs (*34*) and a dependence of the free energy of single mismatches on the distance to a helix end (*15*). One goal of our study was to try to provide insight into the origin of such effects.

Both RNA and DNA Display High Cooperativity Near the End of the Helix. In both RNA and DNA, external registers displayed significant percent effects in the coupling free energy. At low ionic strengths, effects were completely nonadditive, 117 and 94% for AA mismatches in RNA and DNA, respectively, and at high ionic strengths, significant effects persisted, 68 and 74% for AA mismatches in RNA and DNA, respectively (Table 2). Complete nonadditivity strongly supports the notion that the terminal base pair is formed only when the penultimate pair is formed. Indeed, in RNA and DNA at both ionic strengths, changing the GC base pair to an IC base pair at position 1 in the background of the AA mismatch gave effects between −0.24 to 0.42 kcal/mol, suggesting there was no base pair left to break.

Furthermore, this phenomenon does not appear to be dependent on the identity of the penultimate mismatch, as demonstrated by the UU and GG mismatch thermodynamic cycles. In these cases, changing the GC base pair to an IC base pair at position 1 subsequent to the mismatch change resulted in very weak effects ranging between 0.20 and −0.21 kcal/mol. This interpretation is congruent with the high entropic penalty required to initiate a helix in RNA or DNA, causing initiation to be unsuccessful when subsequent propagation is blocked (*14*).

Only RNA Displays High Cooperativity Near the Middle of the Helix. Internal registers exhibited significant effects in coupling free energy only for RNA (Tables 2 and 4), with the effect being strongest for the AA mismatch. The physical basis for internal cooperativity in dsRNA may stem from the bases being held closer together than in dsDNA: 2.9 Å rise/bp for dsRNA versus 3.4 Å rise/bp for dsDNA (*14*). Moreover, dsRNA has greater electrostatic strain than dsDNA. The A-form helix of RNA has a deep and narrow major groove with phosphate groups pointing toward each other. The closest approach of phosphates across the groove, corrected by 5.8 Å for van der Waals radii, is 2.7 Å for A-form dsRNA and 5.7 Å for B-form dsDNA (*14*). These geometrical and electrostatic differences also cause dsRNA to be stiffer than dsDNA, with persistence lengths of 720 and 500 Å, respectively (*14*, *35*). Tighter packing, larger electrostatic strain, and greater stiffness may cause deletion of a functional group to have a greater perturbation on neighboring interactions in dsRNA than in dsDNA.

At the same time, comparatively looser molecular packing may afford dsDNA the opportunity, upon introduction of a mismatch, to refold into a new conformation with similar, or even more favorable, energetics. Moreoever, DNA flexibility is accentuated at higher ionic strengths. For example, transient electric birefringence studies on DNA fragments showed that the persistence length of dsDNA decreases by 31% at higher salt concentrations, consistent with this notion (*36*). Observation of negative coupling internally for DNA at high salt concentrations (Table 2) is consistent with greater backbone flexibility at higher ionic strengths, as are AT to AA changes having diminished effects (by ∼0.65 kcal/mol) at higher ionic strengths in DNA but not RNA.

Large Percent Cooperativity Effects Are Not Tantamount to Large Stability Effects. In RNA, the magnitudes of individual coupling free energy terms for a given nearest-neighbor context were nearly identical internally and externally for the AA mismatch (Table 2). For example, δ_{12} and δ_{45} were −1.68 and −1.73 at low salt concentrations and −0.91 and −1.06 at high salt concentrations, respectively. At the same time, much larger percent cooperativity effects were found for external rather than internal registers. For example, δ_{12} and δ_{45} had percent effects of 117 and 50% at low salt concentrations and 68 and 34% at high salt concentrations, respectively. These observations suggest that externally the AA mismatch causes the complete disruption of a weaker base pair, while internally it causes the partial disruption of stronger base pairs. This is consistent with terminal base pairs being weaker due to fraying (*25*, *37*, *38*).

Compared to those of the AA mismatch, smaller percent effects were observed internally for UU and GG mismatches. For example, δ_{12} and δ_{45} had percent effects of 86 and 26% for UU and 117 and 28% for GG, respectively (Table 4). The smaller internal effects for these two mismatches can be understood in part from noting that the GG mismatch can be accommodated in an A-form helix without major perturbation of the helix (*32*) and that the UU mismatch, being water-bridged, may perturb the helix to an intermediate degree (*31*). In sum, the UU and GG mismatches follow the same general trend as the AA mismatch, with larger

percent effects observed externally than internally, with the even smaller effects internally for the UU and GG mismatches as demonstrated in structural studies. As mentioned in the Results, the smaller internal effects for the GG mismatch are also reasonable on the basis of earlier thermodynamic studies on single mismatches (*15*).

Single substitutions have much larger free energy perturbations internally than externally (e.g., on average, ΔG_{AA} is 4.6 kcal/mol vs 1.7 kcal/mol in RNA). This effect may reflect how well the helix can dissipate the geometric destabilization of a purine-purine mismatch. When the AA mismatch is located penultimate to the base of a helix, the disruption may break only the terminal base pair. Indeed, the coupling of base pair 2 to base pair 1 is larger in magnitude than that to base pair 3, −1.68 and −1.12 kcal/mol, respectively, at low salt concentrations; moreover, the apparent coupling between base pairs 2 and 3 may occur only because position 3 can accommodate a CI pair better when it is at the effective end of a helix.

In contrast, when the AA mismatch is located in the middle of the helix, the perturbations can extend both above and below the mismatch. In the stiff RNA helix, this "rippling effect" may lead to significant total energetic destabilization. For example, base pair 5 couples significantly to its nearest-neighbor base pairs 4 and 6, as well as its next-nearest neighbor, base pair 3, with δ_{45}, δ_{56}, and δ_{35} values of −1.73, −0.85, and −0.79 kcal/mol, respectively, at low salt concentrations. (Differences in magnitude between δ_{45} and δ_{56} may occur because the CG base pair at position 6 has two AU nearest neighbors, while the CG base pair at position 4 has one CG nearest neighbor, which may stiffen the helix and accentuate disruption.)

Last, comparison of δ_{45} and δ_{23} is relevant because base pairs 3 and 4 have nearly identical nearest-neighbor contexts. We found that δ_{45} is significantly larger in magnitude than δ_{23}, −1.73 and −1.12 kcal/mol, respectively, at low salt concentrations, consistent with the notion that the AA mismatch-induced helical disruption is better dissipated when it is located near the terminus of the helix. In sum, the greater energetic perturbation of an internal mismatch appears to be due to the partial disruption of multiple, strong nearest- and next-nearest-neighbor base pairs induced by difficulty in dissipating the geometrical disruption of an AA mismatch defect; the smaller energetic perturbation of an external mismatch appears to be due to the complete disruption of a weak terminal base pair, which may arise because the geometrical disruption of an AA mismatch can be dissipated out the end of the helix.

Implications for Structure Prediction. One of the assumptions of the nearest neighbor model is that the free energy consequence for a given change in sequence, such as insertion of a single mismatch, is independent of its position in the helix. However, in DNA, the AT to AA change is much more penalizing in the internal than the external register, by 1.2 kcal/mol on average. In RNA, the same AU to AA change is even more dependent on helix position, with the internal change 2.9 kcal/mol more penalizing than the external change on average. Clearly, the nearest-neighbor model does not hold in these instances. Curiously, the magnitude of these non-nearest-neighbor effects is relatively independent of ionic strength between 14 and 114 mM, suggesting it will persist at an ionic strength of 1 M where nearest-neighbor parameters are typically measured. Indeed, Kierzek and co-workers reported similar position effects of single mismatches at 1 M NaCl (*15*). A more complete understanding of such phenomena should aid prediction of structure.

Intrinsic Energetic Value of a Hydrogen Bond. Deletion of the 2-amino group in the GC to IC change had relatively minor energetic consequences in DNA. Free energy changes associated with this change were 0.6 and 1.7 kcal/mol for external and internal helical positions, respectively, averaged across ionic strengths (Table 2). A study by Watkins et al. (*39*) found a GC base pair in an internal position was on average 0.84 kcal/mol more stable than a similarly positioned IC base pair in 1 M NaCl, in good agreement with the data presented here.

In the case of RNA, values for the GC to IC change were significantly larger than in DNA, with averages of 1.4 and 3.3 kcal/mol for external and internal helical positions 1 and 4, respectively, averaged across ionic strengths. At the low end of the range is the value for base pair 1 in RNA, which is in good agreement with values previously reported for single GC to IC terminal base pair changes in 1 M NaCl (*22*). At the high end of the range is the value for the GC to IC change at base pair 4. This value is approximately twice the largest value previously reported for an external register (*22*). One interpretation of large observed internal effects is that hydrogen bonds are worth as much as 3.3 kcal/mol inside helices. However, the exceptionally large value of 3.3 kcal/mol is accompanied by a large average δ_{45} value of −1.4 kcal/mol. This suggests instead that the GC to IC change results in the loss of more than just one hydrogen bond (i.e., high cooperativity) and that the intrinsic energetic value of the hydrogen bond is significantly smaller than observed effects, as suggested elsewhere (*23*, *24*, *40*). The molecular origin of the cooperativity between an internal IC and the neighboring base pairs may be hydration effects and will require further investigation.

Conclusions. Comparison of nonadditivity in RNA and DNA secondary structures reveals three classes of behavior. In highly structured loops, RNA is less cooperative than DNA (*26*). In internal helical registers, RNA is more cooperative than DNA. In external helical registers, RNA and DNA both display large cooperativity. Clearly, nonadditivity depends on a number of factors, including the position of the register in the helix or loop, the biopolymer, and the ionic strength. The folding cooperativity appears to have different origins in each case. Higher cooperativity for DNA in loops may be because DNA has fewer interactions causing it to be minimally stable and easily collapsed upon one of the mutations (*26*). Higher cooperativity for RNA internally may be due to tighter packing, which causes greater stiffness and a compromised ability to dissipate geometric perturbation upon mutation. High cooperativity for both polymers externally can be understood in terms of the entropic penalty for helix initiation.

The coupling free energy values reported herein are large in comparison to those from other RNA studies. For example, Klostermeier and Millar (*17*) found maximal coupling free energy values of only 0.6 kcal/mol for tertiary contacts in the hairpin ribozyme, and Silverman and Cech (*41*) found values of ∼0 for tertiary interactions in the *Tetrahymena* group I intron. Apparently, secondary structures display

cooperativity values equal to or greater than those of complex tertiary structures. This may be because tertiary interactions often involve an extensive and overdetermined network of interactions.

These findings should be applicable to numerous biochemical studies involving RNA and DNA, including interpreting effects of naturally occurring helical defects, point mutants, and mismatches on RNA−protein interactions, enzyme function, and RNA and DNA structure prediction. Because bulges and mismatches create effective helix ends (*42*), cooperativity may be dependent on positioning relative to helical defects as well. These results also provide plausible contexts in which to explore pK_a shifting, since higher total cooperativity may mimic structure-forming processes that occur upon proton uptake and A^+•C wobble base pair formation (*30*).

ACKNOWLEDGMENT

We thank Josh Blose, Durga Chadalavada, and Andrea Szakal for comments on the manuscript. We also thank Tobin Sosnick for enlightening conversations.

SUPPORTING INFORMATION AVAILABLE

Sample plots for UV melt experiments, analysis of oligonucleotides by PAGE and TOF-ES mass spectroscopy, and procedures for error propagation. This material is available free of charge via the Internet at http://pubs.acs.org.

REFERENCES

1. Breaker, R. R. (2004) Natural and engineered nucleic acids as tools to explore biology, *Nature 432*, 838−845.
2. Doudna, J. A., and Lorsch, J. R. (2005) Ribozyme catalysis: Not different, just worse, *Nat. Struct. Mol. Biol. 12*, 395−402.
3. Brion, P., and Westhof, E. (1997) Hierarchy and dynamics of RNA folding, *Annu. Rev. Biophys. Biomol. Struct. 26*, 113−137.
4. Tinoco, I., Jr., and Bustamante, C. (1999) How RNA folds, *J. Mol. Biol. 293*, 271−281.
5. Matzke, M. A., and Birchler, J. A. (2005) RNAi-mediated pathways in the nucleus, *Nat. Rev. Genet. 6*, 24−35.
6. Pan, J., and Woodson, S. A. (1998) Folding intermediates of a self-splicing RNA: Mispairing of the catalytic core, *J. Mol. Biol. 280*, 597−609.
7. Treiber, D. K., and Williamson, J. R. (1999) Exposing the kinetic traps in RNA folding, *Curr. Opin. Struct. Biol. 9*, 339−345.
8. Treiber, D. K., and Williamson, J. R. (2001) Beyond kinetic traps in RNA folding, *Curr. Opin. Struct. Biol. 11*, 309−314.
9. Brown, T. S., Chadalavada, D. M., and Bevilacqua, P. C. (2004) Design of a highly reactive HDV ribozyme sequence uncovers facilitation of RNA folding by alternative pairings and physiological ionic strength, *J. Mol. Biol. 341*, 695−712.
10. Russell, R., and Herschlag, D. (2001) Probing the folding landscape of the *Tetrahymena* ribozyme: Commitment to form the native conformation is late in the folding pathway, *J. Mol. Biol. 308*, 839−851.
11. Mathews, D. H., and Turner, D. H. (2006) Prediction of RNA secondary structure by free energy minimization, *Curr. Opin. Struct. Biol. 16*, 268−270.
12. Xia, T., SantaLucia, J., Jr., Burkard, M. E., Kierzek, R., Schroeder, S. J., Jiao, X., Cox, C., and Turner, D. H. (1998) Thermodynamic parameters for an expanded nearest-neighbor model for formation of RNA duplexes with Watson-Crick base pairs, *Biochemistry 37*, 14719−14735.
13. SantaLucia, J., Jr. (1998) A unified view of polymer, dumbbell, and oligonucleotide DNA nearest-neighbor thermodynamics, *Proc. Natl. Acad. Sci. U.S.A. 95*, 1460−1465.
14. Bloomfield, V. A., Crothers, D. M., and Tinoco, I., Jr. (2000) *Nucleic Acids: Structures, Properties, and Functions*, University Science Books, Sausalito, CA.
15. Kierzek, R., Burkard, M. E., and Turner, D. H. (1999) Thermodynamics of single mismatches in RNA duplexes, *Biochemistry 38*, 14214−14223.
16. Di Cera, E. (1998) Site-specific thermodynamics: Understanding cooperativity in molecular recognition, *Chem. Rev. 98*, 1563−1592.
17. Klostermeier, D., and Millar, D. P. (2002) Energetics of hydrogen bond networks in RNA: Hydrogen bonds surrounding G+1 and U42 are the major determinants for the tertiary structure stability of the hairpin ribozyme, *Biochemistry 41*, 14095−14102.
18. Kraut, D. A., Carroll, K. S., and Herschlag, D. (2003) Challenges in enzyme mechanism and energetics, *Annu. Rev. Biochem. 72*, 517−571.
19. Bevilacqua, P. C., Brown, T. S., Nakano, S., and Yajima, R. (2004) Catalytic roles for proton transfer and protonation in ribozymes, *Biopolymers 73*, 90−109.
20. Horovitz, A., and Fersht, A. R. (1990) Strategy for analysing the co-operativity of intramolecular interactions in peptides and proteins, *J. Mol. Biol. 214*, 613−617.
21. Zheng, X., and Bevilacqua, P. C. (2000) Straightening of bulged RNA by the double-stranded RNA-binding domain from the protein kinase PKR, *Proc. Natl. Acad. Sci. U.S.A. 97*, 14162−14167.
22. Turner, D. H., Sugimoto, N., Kierzek, R., and Dreiker, S. D. (1987) Free energy increments for hydrogen bonds in nucleic acid base pairs, *J. Am. Chem. Soc. 109*, 3783−3785.
23. Kool, E. T. (2001) Hydrogen bonding, base stacking, and steric effects in DNA replication, *Annu. Rev. Biophys. Biomol. Struct. 30*, 1−22.
24. Moody, E. M., and Bevilacqua, P. C. (2003) Folding of a stable DNA motif involves a highly cooperative network of interactions, *J. Am. Chem. Soc. 125*, 16285−16293.
25. Moody, E. M., and Bevilacqua, P. C. (2004) Structural and energetic consequences of expanding a highly cooperative stable DNA hairpin loop, *J. Am. Chem. Soc. 126*, 9570−9577.
26. Moody, E. M., Feerrar, J. C., and Bevilacqua, P. C. (2004) Evidence that folding of an RNA tetraloop hairpin is less cooperative than its DNA counterpart, *Biochemistry 43*, 7992−7998.
27. Alberts, B., Bray, D., Lewis, J., Raff, M., Roberts, K., and Watson, J. D. (1994) in *Molecular Biology of the Cell*, pp 508, Garland Publishing, Inc., New York.
28. Turner, D. H., and Bevilacqua, P. C. (1993) Thermodynamic considerations for evolution by RNA, in *The RNA World* (Gesteland, R. F., and Atkins, J. F., Eds.) pp 447−464, Cold Spring Harbor Laboratory Press, Plainview, NY.
29. Proctor, D. J., Ma, H., Kierzek, E., Kierzek, R., Gruebele, M., and Bevilacqua, P. C. (2004) Folding thermodynamics and kinetics of YNMG RNA hairpins: Specific incorporation of 8-bromoguanosine leads to stabilization by enhancement of the folding rate, *Biochemistry 43*, 14004−14014.
30. Moody, E. M., Lecomte, J. T., and Bevilacqua, P. C. (2005) Linkage between proton binding and folding in RNA: A thermodynamic framework and its experimental application for investigating pKa shifting, *RNA 11*, 157−172.
31. Wang, Y. X., Huang, S., and Draper, D. E. (1996) Structure of a U•U pair within a conserved ribosomal RNA hairpin, *Nucleic Acids Res. 24*, 2666−2672.
32. Burkard, M. E., and Turner, D. H. (2000) NMR structures of r(GCAGGCGUGC)$_2$ and determinants of stability for single guanosine-guanosine base pairs, *Biochemistry 39*, 11748−11762.
33. Nagaswamy, U., Larios-Sanz, M., Hury, J., Collins, S., Zhang, Z., Zhao, Q., and Fox, G. E. (2002) NCIR: A database of non-canonical interactions in known RNA structures, *Nucleic Acids Res. 30*, 395−397.
34. He, L., Kierzek, R., SantaLucia, J., Jr., Walter, A. E., and Turner, D. H. (1991) *Biochemistry 30*, 11124−11132.
35. Kebbekus, P., Draper, D. E., and Hagerman, P. (1995) Persistence length of RNA, *Biochemistry 34*, 4354−4357.
36. Lu, Y., Weers, B., and Stellwagen, N. C. (2001) DNA persistence length revisited, *Biopolymers 61*, 261−275.

37. Gueron, M., Kochoyan, M., and Leroy, J. L. (1987) A single mode of DNA base-pair opening drives imino proton exchange, *Nature 328*, 89−92.
38. Wu, M., SantaLucia, J., Jr., and Turner, D. H. (1997) Solution structure of $(rGGCAGGCC)_2$ by two-dimensional NMR and the iterative relaxation matrix approach, *Biochemistry 36*, 4449−4460.
39. Watkins, N. E., Jr., and SantaLucia, J., Jr. (2005) Nearest-neighbor thermodynamics of deoxyinosine pairs in DNA duplexes, *Nucleic Acids Res. 33*, 6258−6267.
40. Kato, Y., Conn, M. M., and Rebek, J., Jr. (1995) Hydrogen bonding in water using synthetic receptors, *Proc. Natl. Acad. Sci. U.S.A. 92*, 1208−1212.
41. Silverman, S. K., and Cech, T. R. (1999) Energetics and cooperativity of tertiary hydrogen bonds in RNA structure, *Biochemistry 38*, 8691−8702.
42. Weeks, K. M., and Crothers, D. M. (1993) Major groove accessibility of RNA, *Science 261*, 1574−1577.

BI061375L